Remote sensing data processing by multivariate regression analysis method for iron mineral resource potential mapping: A case study in the Sarvian area, central Iran

Edris Mansouri[1], Faranak Feizi[2*], Alireza Jafari Rad[1], Mehran Arian[1]

1- Department of Geology, Science and Research branch, Islamic Azad University, Tehran, Iran

2- Department of Mining Engineering, South Tehran branch, Islamic Azad University, Tehran, Iran

*corresponding author: Faranak Feizi

Fax number: +98 021 88830012; Cell: +98 912 3006753; faranakfeizi@gmail.com.

ABSTRACT

This paper uses multivariate regression to create a mathematical model for iron skarn exploration in the Sarvian area, central Iran, using multivariate regression for Mineral Prospectivity Mapping (MPM). The main target of this manuscript is to apply multivariate regression analysis (as a MPM method) to mapping iron outcrops in the northeastern part of the study area in order to discover new iron deposits in other parts of the study area. Two types of multivariate regression models using two linear equations were employed to discover new mineral deposits. Aster satellite images (14 bands) were used as Unique Independent Variables (UIVs), and iron outcrops were mapped as dependent variables for MPM. According to the results of p-value, R^2 and R^2_{adj}, the second regression model (which was a multiples of UIVs) fitted better than other models. The accuracy of the model was confirmed by iron outcrops map and geological observations. Based on field observation, iron mineralization occurs at the contact of limestone and intrusive rocks (skarn type). Iron minerals consist dominantly of magnetite, hematite and goethite.

Key words: Multivariate regression, Mineral Prospectivity Mapping, Iron, Sarvian

1. INTRODUCTION

Preparing the information on an object without touching is called remote sensing. The technology of acquiring data through a device which is located at a distance from the object and the analysis of the data for the purpose of interpreting the physical attributes of the object are two facts of remote sensing (Gupta, 2003).Recently, application of remotely-sensed data in natural resources mapping has been popular. In the other words, applications of remote sensing in geological investigations is the best approach for large scale studies (Melesse et al., 2007). In this

research, we present some of the most commonly used applications of the techniques in mineral resources mapping.

Mineral exploration is a complicated process that involves a focus on delineation of target areas in the search for new mineral deposits (Xiong et al., 2017). The principal aim of mineral investigation in the region of interest is to diagnose futuristic zones and to find new mineral deposits. One way to achieve this aim is using satellite image processing in order to identify Mineral Prospectivity Mapping (MPM) (Carranza, 2008; Abedi et al., 2013; Golshadi et al., 2016 and Feizi et al., 2012).

Mineral prospectivity mapping using 2D geoscientific data, such as geological, geochemical, geophysical and remote sensing data, among others, has been widely used for mineral exploration and targeting for the last 30 years (Li et al., 2015, Abedi et al., 2012; Bonham-Carter and Agterberg, 1990; Carranza, 2009; Carranza and Sadeghi, 2010c; Ford and Blenkinsop, 2008; Lindsay et al., 2014; Lisitsin et al., 2013; Pan and Harris, 2000; Porwal et al., 2010).

The utilization of satellite images for mineral investigation has been extremely effective in indicating out the presence of minerals. Likewise, remote sensing provides a synoptic view, which is useful for identifying and delineation different landscapes, linear features, and structural elements (Feizi and Mansouri, 2013a).

The regression analysis is a statistical process in order to estimating the relationships among variables. There are many techniques for analyzing several variables, when the focus is on the relationship between a dependent variable and one or more independent variables, which the latter case is called multivariate regression analysis. This regression analyses has been utilized as part of numerous logical fields, such as geoscience branches.

Identification of stream sediment anomalies have been used by multiple regression analyses (e.g., Carranza, 2010a; Carranza, 2010b). Likewise, multivariate regression has been effectively utilized by Granian et al. (2015) to display subsurface mineralization from lithogeochemical information. Granian et al. (2015) used four types of multivariate regression models to depict significant surface geochemical anomalies indicating subsurface gold mineralization utilizing borehole data as dependent variables and surface lithogeochemical data as independent variables.

Based on previous work such as Allbed et al., (2012), modelling and mapping of mineral potentials based on satellite image data and processing it based on remote sensing and regression analysis is a promising approach as it facilitates timely detection with a low-cost procedure and allows decision makers to decide what necessary action should be taken as the first step in Mineral Prospectivity Mapping (MPM) field.

The main objective of this research was to use multivariate regression analysis (as a MPM method) to use pixel values from Aster satellite images of the northeastern part of the study area to identify new iron deposits in other parts. Two types of multivariate regression models were used to find new mineral deposits, using pixel values of Aster satellite image bands (14 bands) as Unique Independent Variables (UIVs), and iron outcrop areas (digitized a 1:5000 geology map of the study area and field) data as dependent variables.

This paper uses multivariate regression to develop a useful and precise mathematical model of iron potential zones the region of the interest.

2. METHODOLOGY

2.1. STUDY AREA

The Sarvian area is in the Orumieh-Dokhtar magmatic arc in Central Iran (Fig. 1a). This magmatic arc is the most important metallogenic area inside the district and hosts large metal deposits such as lead, zinc, copper and iron (Feizi et al., 2016 and Feizi et al., 2017).

The study area is dominated by Eocene intrusive rocks and carbonates of the Qom formation. Several types of metal and non-metal mineral ore deposits have, as of now, been reported in the study area. According to the 1:100,000 geological map of Kahak, the lithology of this area includes cream limestone with intercalations of marls (Qom formation), dark green, andesitic-basaltic lava, volcanic breccia, hyaloclastic limestone, green megaporphyritic andesitic-basaltic lava, rhyodacitic domes, tonalite-quartzdiorite, microquartzdiorite-microquartzmonzo-diorite, granite-granodiorite, altered of light green, grey tuff, tuffaceous sandstone and shale with intercalation of nummulitic sandy limestone and andesitic lava, and orbitolina-bearing, thick bedded to massive grey limestone (Aptian–Albian) (Feizi et al., 2016) (Fig. 1b).

Figure 1 is about here.

These relationships are demonstrated by the calcic iron skarn ore (Sarvian mine) in the northeast of study area (Feizi et al., 2017) (Fig. 2). Skarn-type Fe mineralization and alteration are localized along the contact zone between intrusive rocks and carbonate sequences (Zuo et al., 2014).

Figure 2 is about here.

2.2. MULTIVARIATE REGRESSION

Regression analyses is a good statistical tool for analyzing relationships among dependent and independent variables (Granian et al., 2015). In regression analyses, for dependent variables (Y) and independent variables called (x_i), the equation is:

$$Y = f(x_i). \qquad (1)$$

Y can be a linear or non-linear function. For linear regression Y is defined as follows:

$$Y = a_0 + a_1x_1 + a_2x_2 + \cdots + a_ix_i + \varepsilon\,, \quad i = 1,2,\ldots,n. \quad (2)$$

For this function, the constant factor is a_0 , the random error is ε , and the regression coefficients are a_i. If there are n samples in a data set, for each sample t variables were measured. Thus, function (2) is as follows:

$$Y_i = \hat{a}_0 + \hat{a}_1X_{i1} + \hat{a}_2X_{i2} + \cdots + \hat{a}_tX_{it} + \varepsilon_i i = 1,2,\ldots,n. \quad (3)$$

Equation (3) can be re-written as a matrix. The linear function matrix is:

$$[Y] = [X][A] + [\varepsilon]. \quad (4)$$

$$[Y] = \begin{bmatrix} Y_1 \\ Y_2 \\ \cdot \\ : \\ Y_n \end{bmatrix};\ [A] = \begin{bmatrix} \hat{a}_0 \\ \hat{a}_1 \\ \cdot \\ : \\ \hat{a}_t \end{bmatrix};\ [X] = \begin{bmatrix} 1 & X_{11}X_{12} \ldots X_{1t} \\ 1 & X_{21}X_{22} \ldots X_{2t} \\ & \cdot \\ & : \\ 1 & X_{n1}X_{n2} \ldots X_{nt} \end{bmatrix};\ [\varepsilon] = \begin{bmatrix} \varepsilon_1 \\ \epsilon_2 \\ \cdot \\ : \\ \epsilon_n \end{bmatrix}. \quad (5)$$

The least squares technique is used for estimating $[A]$ as the coefficient matrix, as follows:

$$[A] = [\sum\,]^{-1}[C] = ([X]'[X])^{-1}[X]'[Y]. \quad (6)$$

The inverse of variance-covariance samples matrix is $[\sum\,]^{-1}$and the covariance matrix among independent variable and samples is$[C]$. Thus the regression coefficients model is calculated from equation 6.

The following criteria were used for the regression analysis:

1. The variance and the mean of the random error should be a constant value and zero, respectively.

2. The coefficient of determination value (R^2) should be examined. This value is calculated as follows (Granian et al., 2015):

$$R^2 = \frac{\sum_{i=1}^{n}(\hat{Y}_i - \bar{Y})^2}{\sum_{i=1}^{n}(Y_i - \bar{Y})^2} = 1 - \frac{\sum_{i=1}^{n}(Y_i - \hat{Y}_i)^2}{\sum_{i=1}^{n}(Y_i - \bar{Y})^2}. \quad (7)$$

The mean of the variable ($\bar{Y}$), value of the ith sample (Y_i) and estimated value of the ith sample ($\hat{Y}_i$) for dependent variables were used in equation 7. The calculated R^2 value determined within [0, 1] range. The value of R^2 is close to 1 for well fitted models.

1. Given the fact that adding independent variables to the model will increase the R^2 value, the adjusted determination coefficient (R^2_{adj}) is defined as follows (Granian et al., 2015):

$$R^2_{adjusted} = 1 - \frac{n-1}{n-t}(1 - R^2). \quad (8)$$

As it was mentioned, n is number of samples (or data) and t is the number of variables (or regression coefficients). If a set of explanatory variables are introduced into a regression one at a time, with the R^2_{adj}computed each time, the level at which R^2_{adj}reaches a maximum, and decreases afterward, would be a well fitted model.

2. In regression analyses, the model should be fitted to the data. Accordingly, the p-value of the regression model in the analysis of variance (ANOVA) test should be acceptable (less than or equal to 0.05). Calculating the p-value of final coefficients for each model, may also help optimize and improve the model. This criterion could be applied after choosing the best model.

3. DATA COLLECTION

There are several iron ore bodies and one iron mine in the northeastern Sarvian study area. The regional geological conditions of the area, suggest that the Sarvian iron mine is a good model for exploring the surrounding area. In this paper, a geology map of the mine is used as a training area for satellite imagery. In the training area, this method can model the iron outcrops (a dependent variable) based on Aster satellite image bands (independent variables) (Fig. 3).

Figure 3 is about here.

3.1. REMOTE SENSING DATA (INDEPENDENT VARIABLES)

The ASTER sensor was launched in December 1999 on board the Earth Observation System (EOS) US Terra satellite. ASTER provides high-resolution images of the land surface, water, ice, and clouds using three separate sensor subsystems covering 14 multi-spectral bands from visible to thermal infrared (Table 1). Resolutions are 15m, 30m, and 90m in the Visible and Near Infrared (VNIR), Shortwave Infrared (SWIR), and Thermal Infrared (TIR), respectively. For more information see Feizi and Mansouri, (2013b) and Mansouri and Feizi, (2016).

Several factors influence the signal measured at the sensor, for example, radiometric calibration, and atmospheric and topographical effects. In this way, Aster data were analysed using ENVI5.1 software to provide information such as wavelength, dark subtract and log residuals which are basic for multispectral analyses (Mansouri et al., 2015).

In this study after corrections, the pixel size of SWIR and TIR bands based on VNIR3 band (Panchromatic band) was converted to 15 m. The layer stacking function was then used to build a new multiband file from georeferenced images of various pixel sizes, extents, and projections.

Table 1 is about here.

3.2. MAPPING OF IRON OUPCROPS (DEPENDENT VARIABLE)

There are several iron veins and outcrops around the iron ore skarn mine in the north-eastern part of the Sarvian area. Iron outcrops in the training area were mapped using a geological map at a scale of 1:1000 of the iron ore deposit. The map was then field checked. The shape file layer of iron outcrops was converted to a raster file with a pixel size of 15 m.

4. RESULTS AND DISCUSSION

Multiple, factorial, polynomial and response surface regressions have been utilized in many fields including the geosciences (e.g. Granian et al., 2015). In this study; Model 1 (Y_1) was generated as a multiple linear regression model and Model 2 (Y_2) was created from Y_1 plus many UIVs. The formulas for the two models are presented in Table 2. Thus, two linear equations (Y_1 and Y_2) were used to discover new mineral deposits, using pixel values from ASTER satellite data as independent variables and a map of iron outcrops as dependent variables. Of The two models proposed in this paper, model 2 has 106 coefficients (14 for UIVs, 1 as constant, 91 for multiples of UIVs) and model 1 has 15 coefficients (14 for UIVs, 1 as constant, 0 for multiples and exponents of UIVs) (Table 2).

Table 2 is about here.

Regression analyses were performed to assess the models in Table 2, and the critical criteria mentioned above, were examined. The values of the R^2 , R^2_{adj} and p-value from the ANOVA test of 2 multivariate regression models are provided in Table 3.

Table 3 is about here.

Table 4 presents the calculated coefficients of independent variables in regression models. Excluded independent variables are not mentioned in Table 4. Excluded variables were those that had no effect on iron mineralization and the mapped distribution of iron outcrops.

Table 4 is about here.

We used several criteria to review the differences between the two models. Firstly, the variance and the mean of the random error were acceptable for both models. Secondly, based on Table 4, the p-values of ANOVA test of the two models were equal to 0. For regression models, the acceptable p-value should be less than or equal to 0.05. Thus, this criterion confirmed the validity of the models without specifying the most appropriate model.

The value of R^2 is close to 1 for well fitted models. The R^2 values of regression models are presented in Table 3. Model Y1 has a lower R_2 than Y_2. Thus, the Y_2 model is better than the Y_1 model.

Because adding independent variables to the model will increasing the R^2 value, the R^2_{adj} value should be checked. The R^2_{adj} values of regression models are presented in Table 3. As mentioned above, if a set of variables are introduced into a regression, with the R^2_{adj}computed each time, the level at which R^2_{adj}reaches a maximum, and decreases afterward, would be a well-fitted model. So, according to Table 3, Y_2 is the fitted model versus other models. Thus, Y_2 regression model is the most appropriate model for Mineral Prospectivity Mapping.

Thus according to the results of p-value (ANOVA test), R^2 and R^2_{adj}, the second regression model (Y_2) would be the fitted model versus other models. For generating a mineral prospectivity map the model Y_2 was implemented in ArcGIS using the raster calculator tool. The normalized mineral prospectivity map of the study area is presented in Fig. 4.

Figure 4 is about here.

To assess the accuracy of the selected model, the created prospectivity map was checked against the iron outcrops map in the northeastern part of the study area (Fig. 5). The locations of iron outcrops is in close agreement with predictions from the mineral prospectivity map. In addition three target areas with very high potential were checked for iron outcrops and the prospectivity map was confirmed by geological observations (Fig. 6). Based on field observation iron mineralization occurs at contacts between limestone and intrusive rocks (skarn type). Iron mineralizations consists dominantly of magnetite, hematite and goethite. Therefore, the accuracy of the mineral prospectivity map is confirmed in the Sarvian area.

Figure 5 is about here.

Figure 6 is about here.

5. CONCLUSION

The conclusions of this manuscript are as follows.

1) The regression analysis is an appropriate and direct method for MPM by satellite images data. In this paper, the output of processed satellite image using regression analysis indicates the iron potential zones accurately.

2) The application of multivariate regression analysis (as a MPM method) was confirmed in the Sarvian area. This paper used multivariate regression to create a mathematical model (with reasonable accuracy) for iron mineral exploration in the region of interest.

3) Two types of multivariate regression models, as two linear equations, were employed to discover new mineral deposits. According to the results of p-value, R^2 and R^2_{adj}, the second regression model best fitted observations.

4) The accuracy of the model was confirmed by iron outcrops mapping and geological observations. Based on field observation iron mineralization occurs in contacts between limestone and intrusive rocks (skarn type). Iron mineralization consists dominantly of magnetite, hematite and goethite.

5) The results demonstrate that modelling and mapping satellite images data based on regression analysis and remote sensing data is an efficient approach, as it facilitates timely detection with a low-cost procedure and allows decision makers to decide what necessary action should be taken as the first step in Mineral Prospectivity Mapping (MPM) field.

6) Regression analysis method is a subset of supervised classification due to the mentioned procedure. In this method, target spectrums of training area are used for modeling and MPM.

ACKNOWLEDGEMENTS

The authors would like to thank Amirabbas KarbalaeiRamezanali for his helpful suggestions.

REFRENCES

Abedi, M., Torabi, S.A., Norouzi, G.-H., Hamzeh,M.: ELECTRE III: a knowledge-driven method for integration of geophysical data with geological and geochemical data in mineral prospectivity mapping. J. Appl. Geophys. 87, 9–18, 2012.

Abedi, M., Torabi, S.A. and Norouzi, G.H.: Application of fuzzy AHP method to integrate geophysical data in a prospect scale, a case study: Seridune copper deposit. Bollettino di Geofisica Teorica, 54, 145–164, 2013.

Abrams, M.: The Advanced Spaceborne Thermal Emission and Reflection Radiometer (ASTER): Data products for the high spatial resolution imager on NASA's Terra platform, International Journal of Remote Sensing, 21, 5, 847-859, 2000.

Allbed, A., Kumar, L., and Sinha, P.: Mapping and Modelling Spatial Variation in Soil Salinity in the Al Hassa Oasis Based on Remote Sensing Indicators and Regression Techniques, Remote Sens. 6, 1137-1157; 2014.

Bonham-Carter, G., Agterberg, F.: Application of amicrocomputer-based geographic information system to mineral potential mapping. Microcomput. Geol. 2, 49–74, 1990.

Carranza, E.J.M.: Geochemical anomaly and mineral prospectivity mapping in GIS, Handbook of Exploration Environmental Geochemistry. Elsevier, Amsterdam, 368 p, 2008.

Carranza, E., Geochemical Anomaly and Mineral Prospectivity Mapping in GIS. Elsevier Science Ltd, Oxford, pp. 351, 2009.

Carranza, E.J.M.: Catchment basin modelling of stream sediment anomalies revisited: incorporation of EDA and fractal analysis. Geochemistry: Exploration, Environment, Analysis, 10, 365–381, 2010a.

Carranza, E.J.M.: Mapping of anomalies in continuous and discrete fields of stream sediment geochemical landscapes. Geochemistry: Exploration, Environment, Analysis, 10, 171–187, 2010b.

Carranza, E.J.M., Sadeghi, M.: Predictive mapping of prospectivity and quantitative estimation of undiscovered VMS deposits in Skellefte district (Sweden). Ore Geol. Rev. 38, 219–241, 2010c.

Feizi, F. and Mansouri, E.: Identification of Alteration Zones with Using ASTER Data in A Part of Qom Province, Central Iran. Journal of Basic and Applied Scientific Research, 2, 73–84, 2012.

Feizi, F. and Mansouri, E.: Separation of Alteration Zones on ASTER Data and Integration with Drainage Geochemical Maps in Soltanieh, Northern Iran. Open Journal of Geology, 3, 134–142, 2013a.

Feizi, F. and Mansouri, E.: Introducing the Iron Potential Zones Using Remote Sensing Studies in South of Qom Province, Iran. Open Journal of Geology, 3, 278–286, 2013b.

Feizi, F., Mansouri, E. and KarbalaeiRamezanali, A.: Prospecting of Au by Remote Sensing and Geochemical Data Processing Using Fractal Modelling in Shishe-Botagh, Area (NW Iran). Journal of the Indian Society of Remote Sensing, 44, 539–552, 2016.

Feizi, F., KarbalaeiRamezanali, A. and Mansouri, E.: Calcic iron skarn prospectivity mapping based on fuzzy AHP method, a case Study in Varan area, Markazi province, Iran. Geosciences Journal, 21, 123–136, 2017.

Ford, A. and Blenkinsop, T.G.: Combining fractal analysis of mineral deposit clustering with weights of evidence to evaluate patterns of mineralization: application to copper deposits of the Mount Isa Inlier, NW Queensland, Australia. Ore Geol. Rev. 33, 435–450, 2008.

Granian, H., Tabatabaei, S. H., Asadi, H. H. and Carranza, E. J. M.: Multivariate regression analysis of lithogeochemical data to model subsurface mineralization: a case study from the Sari Gunay epithermal gold deposit, NW Iran. Journal of Geochemical Exploration, 148, 249–258, 2015.

Golshadi, Z., KarbalaeiRamezanali, A. and Kafaei, K.: Interpretation of magnetic data in the Chenar-e Olya area of Asadabad, Hamedan, Iran, using analytic signal, Euler deconvolution, horizontal gradient and tilt derivative methods. Bollettino di Geofisica Teorica ed Applicata, 57, 329–342, 2016.

Gupta, R. P.: Remote sensing geology, Berlin, Heidelberg: Springer Berlin Heidelberg: Imprint: Springer, 2003.

Li, X., Yuan, F., Zhang, M., Jia, C., Jowitt, S.M., Ord, A., Zheng, T., Hu, X., Li, Y.: Three-dimensional mineral prospectivity modeling for targeting of concealed mineralization within the Zhonggu iron orefield, Ningwu Basin, China, Ore Geology Reviews, doi: 10.1016/j.oregeorev.2015.06.001, 2015.

Lindsay, M.D., Betts, P.G., Ailleres, L.: Data fusion and porphyry copper prospectivity models, southeastern Arizona. Ore Geol. Rev. 61, 120–140, 2014.

Lisitsin, V., González-Álvarez, I., Porwal, A.: Regional prospectivity analysis for hydrothermal-remobilised nickel mineral systems in western Victoria, Australia. Ore Geol. Rev. 52, 100–112, 2013.

Mansouri, E., Feizi, F. and KarbalaeiRamezanali, A.: Identification of magnetic anomalies based on ground magnetic data analysis using multifractal modelling: a case study in Qoja-Kandi, East Azerbaijan Province, Iran. Nonlinear Processes in Geophysics, 22, 579–587, 2015.

Mansouri, E., Feizi, F.: Introducing Au potential areas, using remote sensing and geochemical data processing using fractal method in Chartagh, western Azarbijan – Iran, E. Archive of Mining Sciences, Vol., No 2, 397–414, 2016.

Melesse, A. M., Weng, Q., Thenkabail, P. S. and Senay, G. B.: Remote Sensing Sensors and Applications in Environmental Resources Mapping and Modelling, Sensors, 7, 3209-3241, 2007.

Pan, G., Harris, D.P.: Information Synthesis for Mineral Exploration. Oxford University Press, New York, pp. 461 , 2000.

Porwal, A., González-Álvarez, I., Markwitz, V., McCuaig, T., Mamuse, A.: Weights-of-evidence and logistic regression modeling ofmagmatic nickel sulfide prospectivity in the Yilgarn Craton, Western Australia. Ore Geol. Rev. 38, 184–196, 2010.

Xiong, Y., Zuo, R.: Effects of misclassification costs on mapping mineral prospectivity, Ore Geology Reviews, doi: 10.1016/j.oregeorev.2016.11.014, 2017.

Zuo, R., Zhang, Z., Zhang, D., Carranza, E.J.M. and Wang, H.: Evaluation of uncertainty in mineral prospectivity mapping due to missing evidence: a case study with skarn-type Fe deposits in Southwestern Fujian Province, China, Ore Geology Reviews, doi: 10.1016/j.oregeorev.2014.09.024, 2014.

Table 1. Wavelength ranges and spatial resolutions of ASTER bands (Abrams, 2000).

Module	VNIR	SWIR	TIR
Spectral bandwidth (μm)	Band 1 0.52 - 0.60	Band 4 1.650 - 1.700	Band 10 8.125 - 8.475
	Band 2 0.63 - 0.69	Band 5 2.145 - 2.185	Band 11 8.475 - 8.825
	Band 3 N 0.78 - 0.86	Band 6 2.185 - 2.225	Band 12 8.925 - 9.275
	Band 3 B 0.78 - 0.86 (backward looking)	Band 7 2.235 - 2.285	Band 13 10.25 - 10.95
		Band 8 2.295 - 2.395	Band 14 10.95 - 11.65
		Band 9 2.360 - 2.430	
Spatial resolution (m)	15	30	90

Table2. Formula of regression models used for Aster satellite image bands

Types of Regression	Number of coefficients	Formula
First-Degree	15	$Y_1 = a_0 + a_1x_1 + a_2x_2 + \cdots + a_{14}x_{14}$
First-Degree	106	$Y_2 = Y_1 + a_{15}x_1x_2 + a_{16}x_1x_3 + \cdots + a_{27}x_1x_{14} + a_{28}x_2x_3 + a_{29}x_2x_4 + \cdots + a_{39}x_2x_{14} + a_{40}x_3x_4 + a_{41}x_3x_5 + \cdots + a_{50}x_3x_{14} + a_{51}x_4x_5 + \cdots + a_{60}x_4x_{14} + a_{61}x_5x_6 + \cdots + a_{69}x_5x_{14} + a_{70}x_6x_7 + \cdots + a_{77}x_6x_{14} + a_{78}x_7x_8 + \cdots + a_{84}x_7x_{14} + a_{85}x_8x_9 + \cdots + a_{90}x_8x_{14} + a_{91}x_9x_{10} + \cdots + a_{96}x_9x_{14} + a_{97}x_{10}x_{11} + \cdots + a_{100}x_{10}x_{14} + a_{101}x_{11}x_{12+\cdots+}a_{103}x_{11}x_{14} + a_{104}x_{12}x_{13} + a_{105}x_{12}x_{14} + a_{106}x_{13}x_{14}$

Table 3. The values for R^2 , R^2_{adj} and p-value of ANOVA test of 2 multivariate regression models

Models	R^2	R^2_{adj}	p-value (ANOVA)
Y_1	0.738	0.715	0
Y_2	0.847	0.829	0

Table 4. The calculated coefficients of regression models 1 and 2.

Model 1		**Model 2**	
variables	Coefficients (a_i)	variables	Coefficients (a_i)
CST	0.275	CST	0.677
$\boldsymbol{x_1}$	-0.01	x_1	-0.014
$\boldsymbol{x_2}$	-0.12	x_2	-0.019
$\boldsymbol{x_3}$	-0.019	x_3	-0.045
$\boldsymbol{x_4}$	0.003	x_4	0.022
$\boldsymbol{x_5}$	-0.006	x_5	-0.017
$\boldsymbol{x_6}$	-0.005	x_6	-0.001
$\boldsymbol{x_7}$	-	x_7	-
$\boldsymbol{x_8}$	-0.004	$\boldsymbol{x_8}$	-0.02
$\boldsymbol{x_9}$	-0.005	$\boldsymbol{x_9}$	-0.006
$\boldsymbol{x_{10}}$	0.009	$\boldsymbol{x_{10}}$	-0.014
$\boldsymbol{x_{11}}$	0.005	$\boldsymbol{x_{11}}$	0.024
$\boldsymbol{x_{12}}$	0.016	$\boldsymbol{x_{12}}$	0.024
$\boldsymbol{x_{13}}$	0.002	$\boldsymbol{x_{13}}$	0.018
$\boldsymbol{x_{14}}$	0.022	$\boldsymbol{x_{14}}$	0.036
-	-	x_1x_4	-0.0009
-	-	x_1x_6	-0.0002
-	-	x_4x_9	-0.0009
-	-	x_7x_8	0.00082

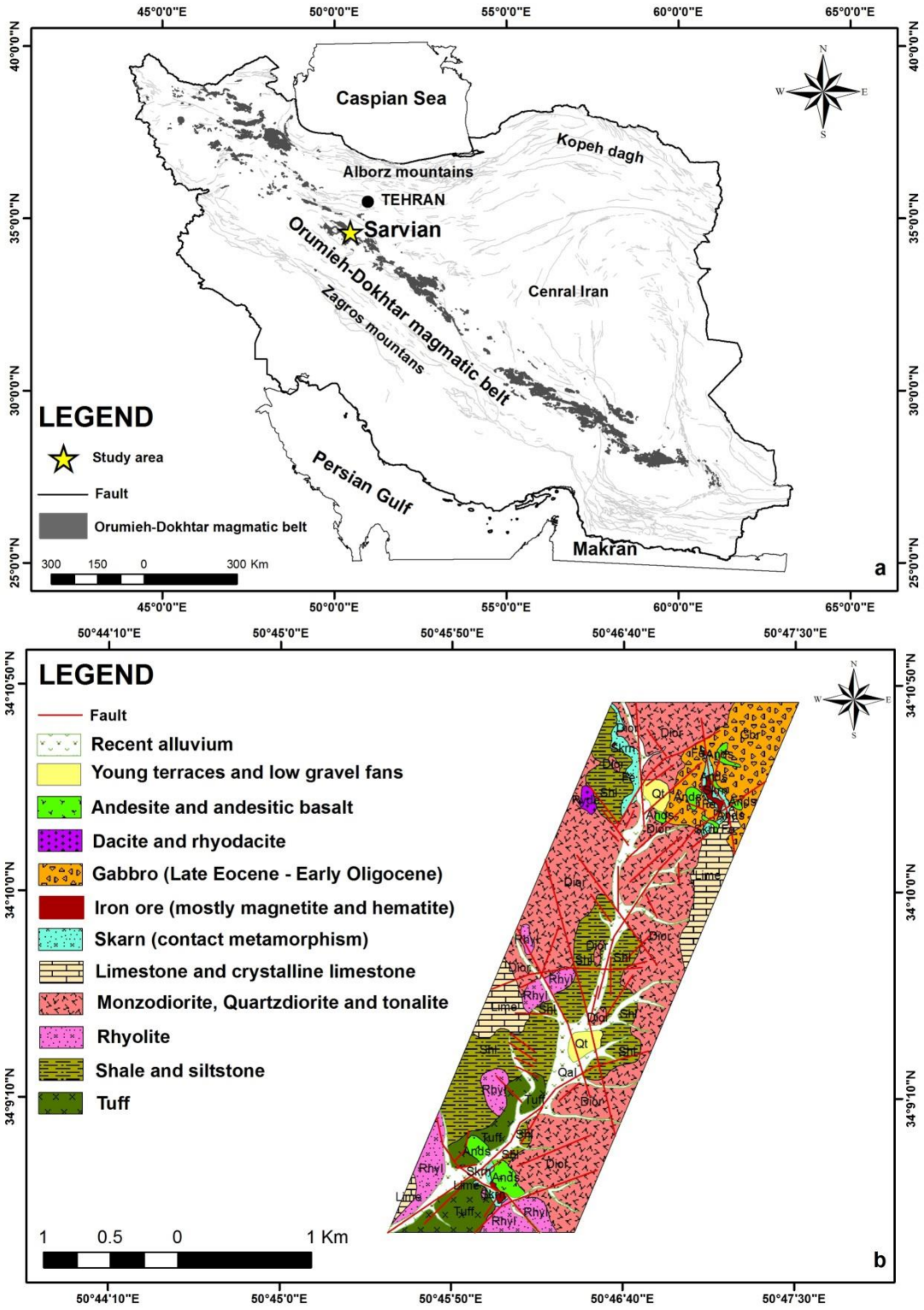

Fig. 1. a) The location of the Sarvian area in the Orumieh–Dokhtar magmatic belt, Iran **b)** Geological map of the Sarvian area (scale 1:25000).

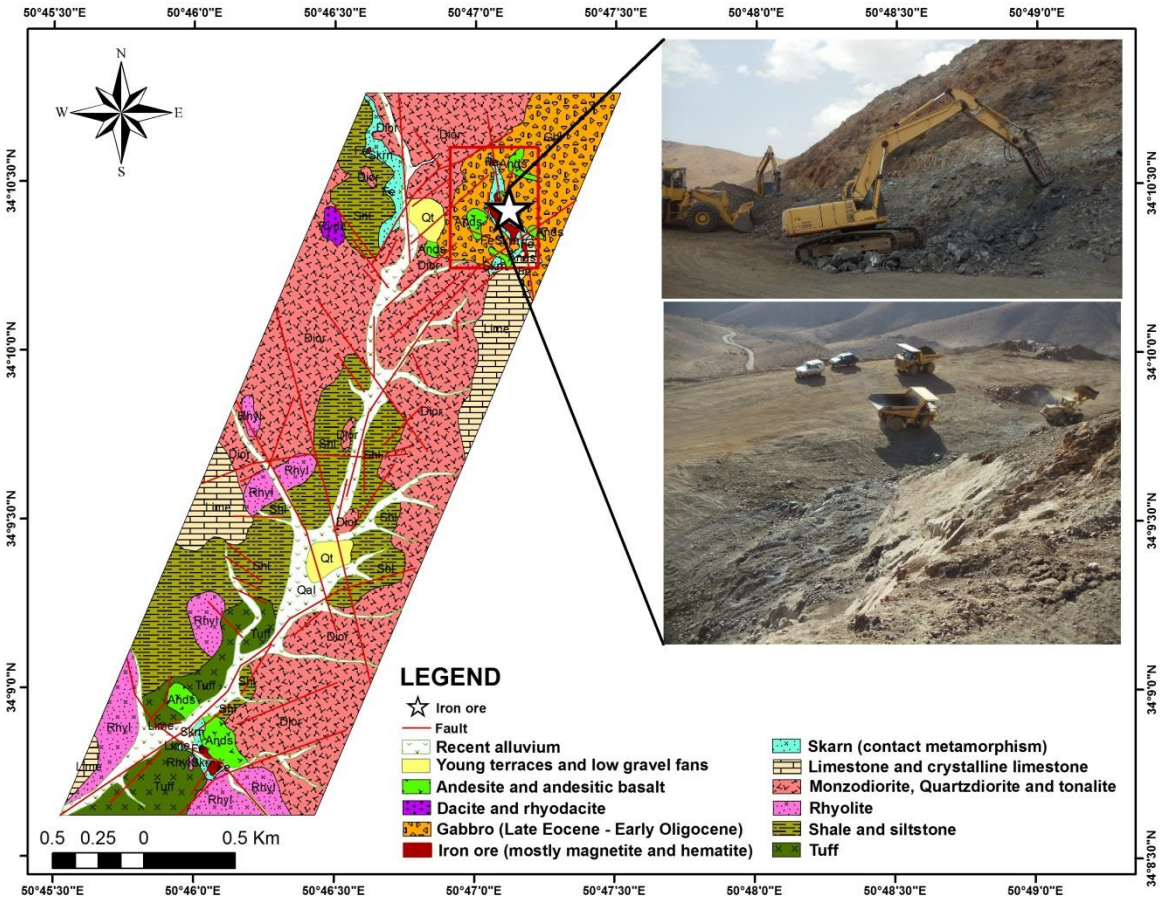

Fig. 2. Location of the Sarvian iron mine in the study area.

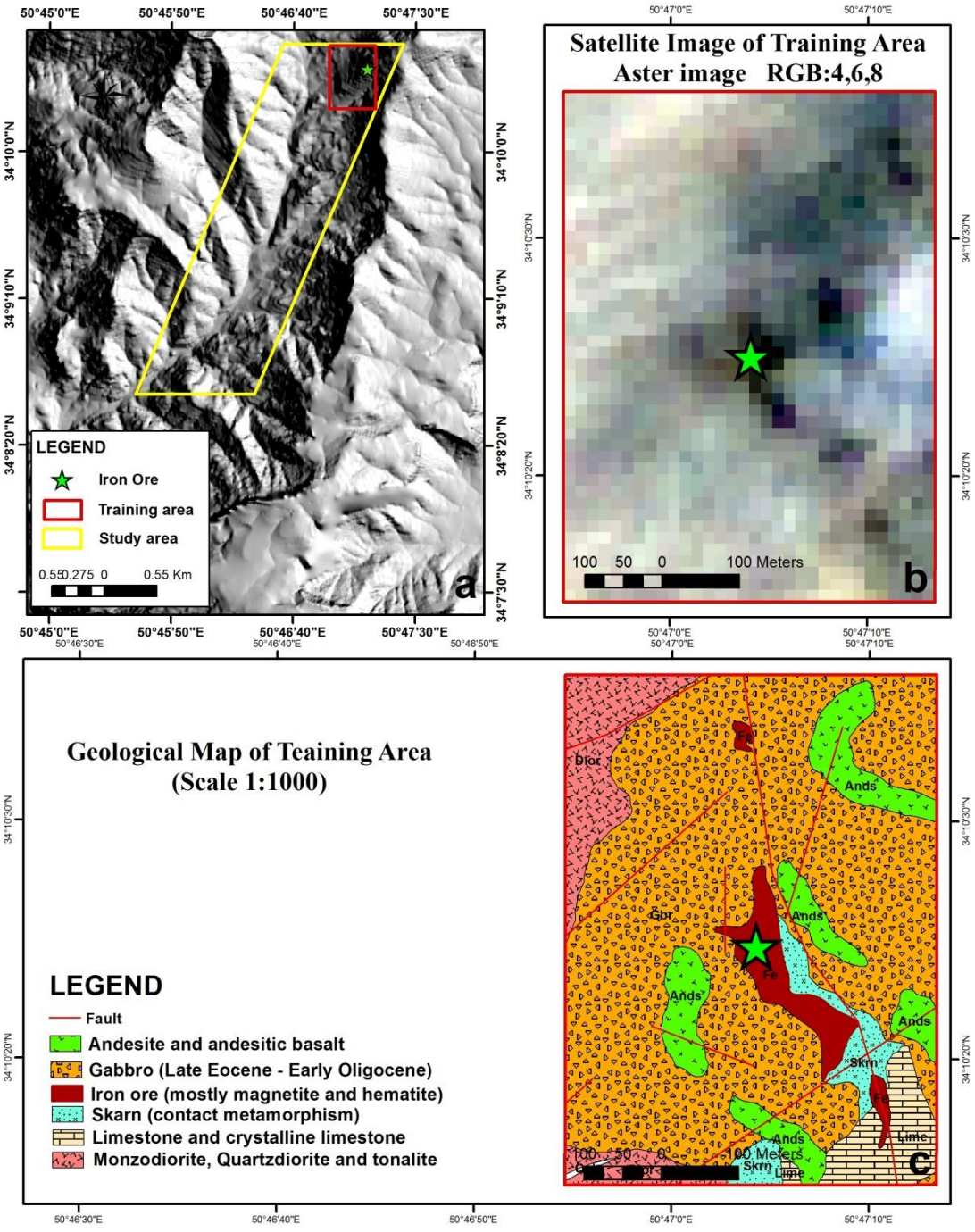

Fig. 3. a) Location of training area in the study area. b) Aster satellite image in the training area (RGB:4,6,8). c) Geological map (scale 1:1000) of training area.

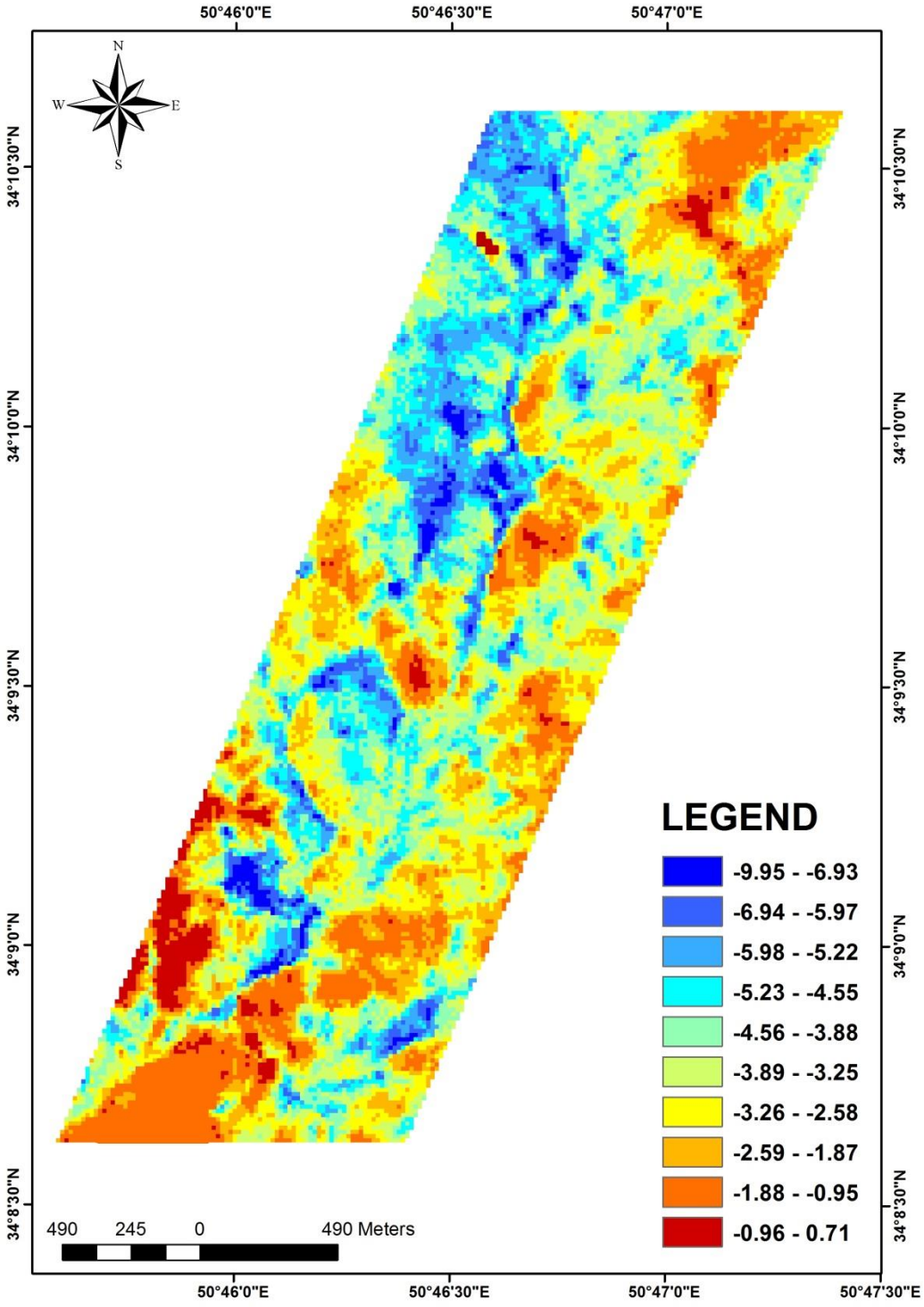

Fig. 4. Mineral prospectivity map of the Sarvian area.

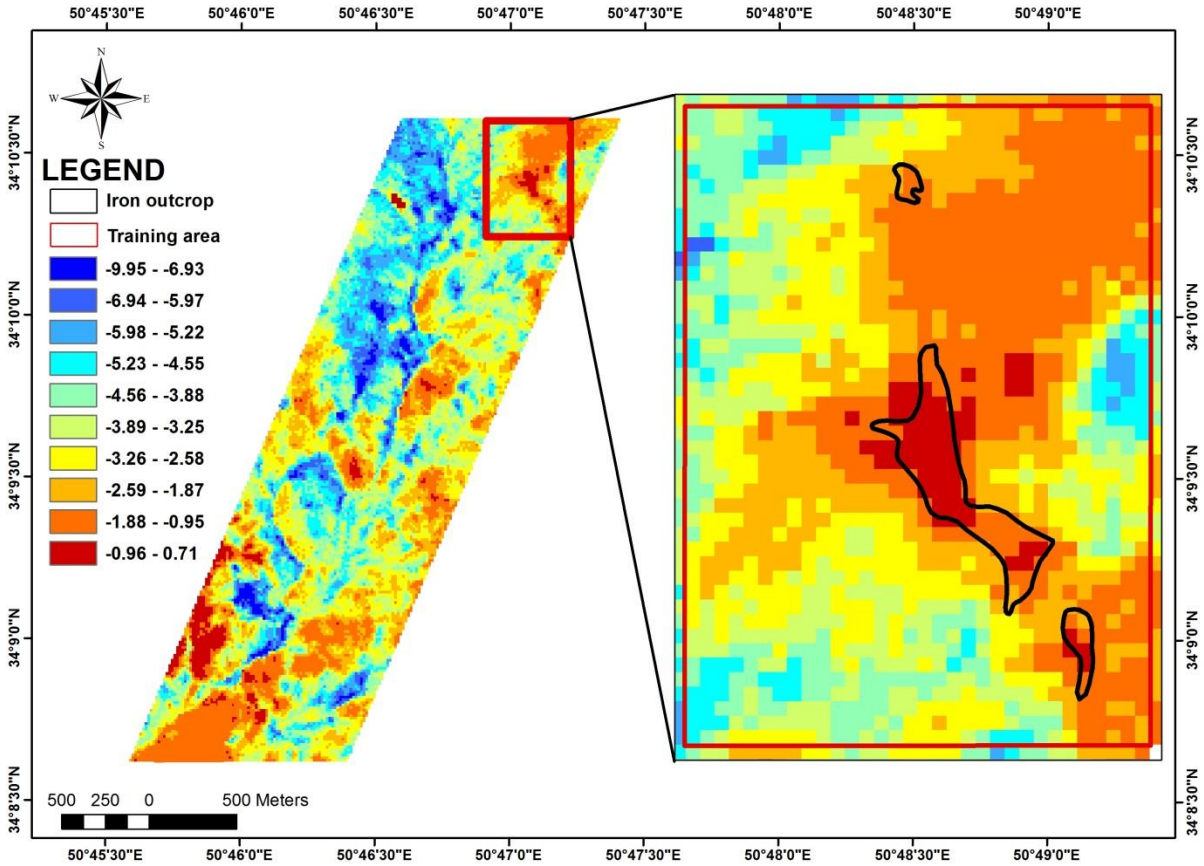

Fig. 5. Mineral prospectivity map of the Sarvian area which confirmed by iron outcrops.

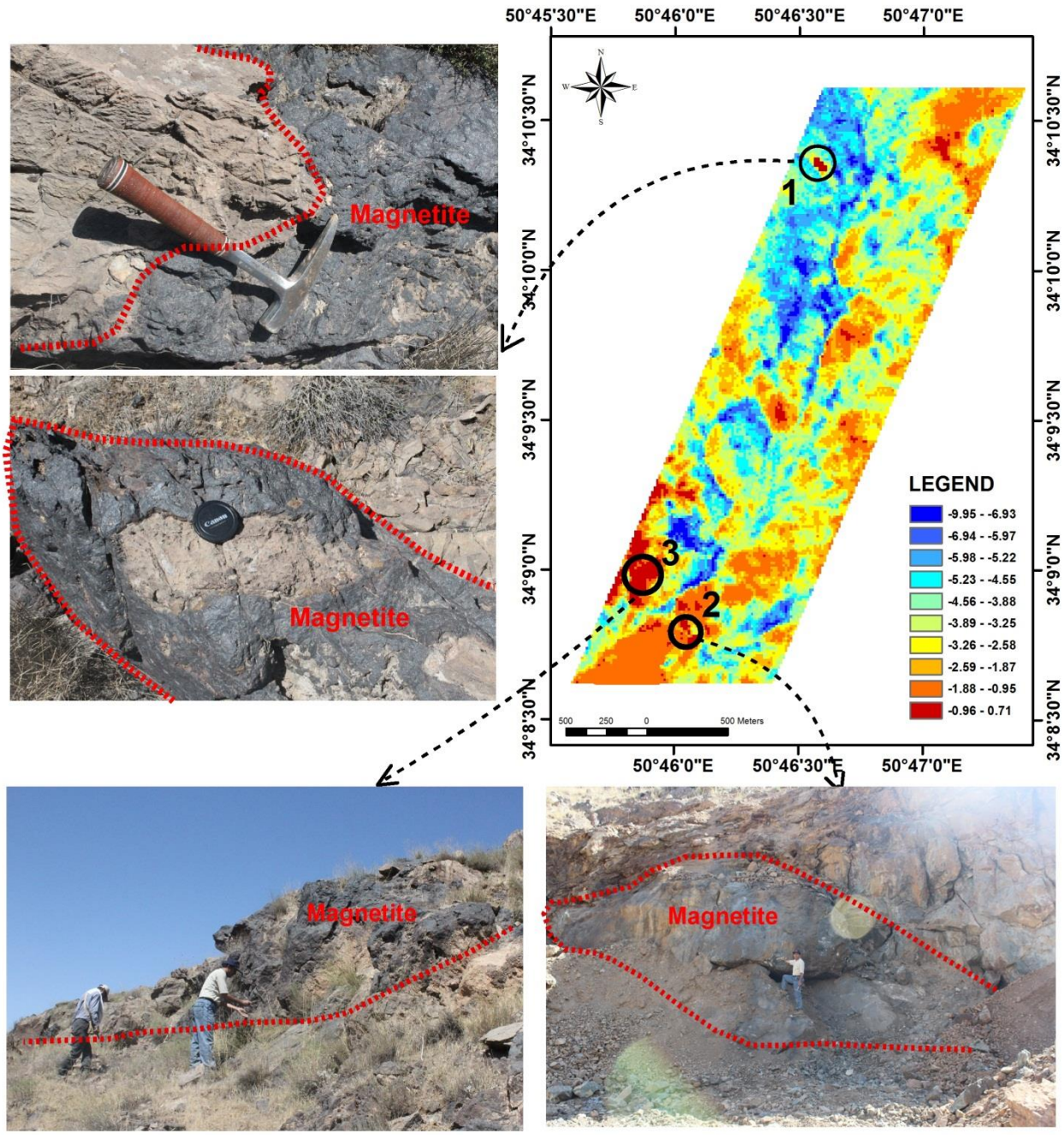

Fig. 6. Mineral prospectivity map of the Sarvian area which confirmed by check field of three target areas.